AGU ADVANCING EARTH AND SPACE SCIENCE

Geophysical Research Letters

RESEARCH LETTER
10.1029/2020GL088648

Triggering the Indian Ocean Dipole From the Southern Hemisphere

Lian-Yi Zhang[1,2,3,4], **Yan Du**[1,2,3], **Wenju Cai**[5,6], **Zesheng Chen**[1,3], **Tomoki Tozuka**[4], **and Jin-Yi Yu**[7]

[1]State Key Laboratory of Tropical Oceanography, South China Sea Institute of Oceanology, and China-Pakistan Joint Research Center on Earth Sciences, CAS, Guangzhou, China, [2]College of Earth and Planetary Sciences, University of Chinese Academy of Sciences, Beijing, China, [3]Southern Marine Science and Engineering Guangdong Laboratory, Guangzhou, China, [4]Department of Earth and Planetary Science, The University of Tokyo, Tokyo, Japan, [5]Key Laboratory of Physical Oceanography, Institute for Advanced Ocean Studies, Ocean University of China and Qingdao National Laboratory for Marine Science and Technology, Qingdao, China, [6]Centre for Southern Hemisphere Oceans Research (CSHOR), CSIRO Oceans and Atmosphere, Hobart, Tasmania, Australia, [7]Department of Earth System Science, University of California, Irvine, CA, USA

Key Points:
- A triggering mechanism of the IOD originated from the Southern Hemisphere is identified
- The Southern Hemisphere Mechanism is independent from ENSO and associated with subtropical and high-latitude climatic variability
- The joint effects of such mechanism and ENSO produce different characteristics of the IOD

Supporting Information:
- Supporting Information S1

Correspondence to:
Y. Du,
duyan@scsio.ac.cn

Citation:
Zhang, L.-Y., Du, Y., Cai, W., Chen, Z., Tozuka, T., & Yu, J.-Y. (2020). Triggering the Indian Ocean Dipole from the Southern Hemisphere. *Geophysical Research Letters*, *47*, e2020GL088648. https://doi.org/10.1029/2020GL088648

Received 29 APR 2020
Accepted 16 JUL 2020

Abstract This study identifies a new triggering mechanism of the Indian Ocean Dipole (IOD) from the Southern Hemisphere. This mechanism is independent from the El Niño-Southern Oscillation (ENSO) and tends to induce the IOD before its canonical peak season. The joint effects of this mechanism and ENSO may explain different lifetimes and strengths of the IOD. During its positive phase, development of sea surface temperature cold anomalies commences in the southern Indian Ocean, accompanied by an anomalous subtropical high system and anomalous southeasterly winds. The eastward movement of these anomalies enhances the monsoon off Sumatra-Java during May–August, leading to an early positive IOD onset. The pressure variability in the subtropical area is related with the Southern Annular Mode, suggesting a teleconnection between high-latitude and midlatitude climate that can further affect the tropics. To include the subtropical signals may help model prediction of the IOD event.

Plain Language Summary An Indian Ocean Dipole (IOD) at its positive phase featuring anomalously high and low sea surface temperature (SST) in the west and east equatorial Indian Ocean, respectively, shifts atmosphere convection westward, causing severe floods and droughts in surrounding west and east Indian Ocean-rim regions. Known triggering mechanisms, such as the external El Niño-Southern Oscillation (ENSO), cannot explain development or intensity of many IOD events. Here we find a novel triggering mechanism of the IOD from the Southern Hemisphere, in which the subtropical high pressure and wind anomalies forcing cool SST anomalies evolve to trigger onset of an IOD event via enhancing the monsoon off Sumatra-Java. This Southern Hemisphere Mechanism can operate independently from the ENSO and commences earlier than the ENSO forcing, thus providing explanation of different IOD characteristics and a longer prediction lead time.

1. Introduction

As a major intrinsic climate mode in the tropical Indian Ocean (IO), the Indian Ocean Dipole (IOD) has great impacts not only on the IO rim countries but also over the globe (Cai, Cowan, & Raupach, 2009; Endo & Tozuka, 2015; Izumo et al., 2010; Qiu et al., 2014; Saji & Yamagata, 2003). During a positive IOD event, sea surface temperature (SST) anomalously cools in the equatorial eastern IO while warms in the equatorial western IO; anomalous easterly wind prevails in the equatorial IO driven by the zonal pressure gradient, following the Bjerknes positive feedback (Bjerknes, 1969; Delman et al., 2016; Drbohlav et al., 2007; Saji et al., 1999; Webster et al., 1999; Yu et al., 2005). It leads to severe flood in East Africa and drought in the Indonesian Archipelago owing to a westward movement of the atmospheric convection (Behera et al., 1999; Vinayachandran et al., 1999).

There are various triggering mechanisms of the IOD such as the El Niño-Southern Oscillation (ENSO) (Annamalai et al., 2003; Ashok et al., 2003; Guo et al., 2015) and Madden Julian Oscillation (Rao et al., 2008). All these factors can be categorized as the external forcing or internal forcing within the IO (Yang et al., 2015). An El Niño is considered as the major external forcing to the positive IOD, since it weakens the Walker

Circulation over the Indo-Pacific region (Annamalai et al., 2003; Cai et al., 2013; Yu et al., 2005). When an El Niño event develops, corresponding to the SST change in the Pacific, the deep convection over the Maritime Continent weakens, increasing the sea level pressure (SLP) there (Annamalai et al., 2010). The associated anomalous pressure gradient forces easterly wind anomalies over the equatorial IO, which replaces the weak climatological westerlies (Li et al., 2003; Meyers et al., 2007). The El Niño thus can trigger a positive IOD event. However, the IOD can also develop independently from the ENSO (Behera et al., 2006; Sun et al., 2015). For example, three positive IOD events consecutively occurred in 2006–2008, while the Pacific featured weak La Niña conditions in 2007–2008 that would impede positive IOD developments (Cai, Pan, et al., 2009; Luo et al., 2008; Rao et al., 2008). Previous studies also illustrated that internal variabilities of the IO such as the anomalous equatorial easterly wind and oceanic waves play roles in triggering the IOD in those independent cases (Cai & Qiu, 2013; Crétat et al., 2017; Moum et al., 2014; Yang et al., 2015).

Although we have good understandings on such internal forcings in the tropical IO, whether and how the subtropical IO affects the IOD is still unclear, especially from the southern IO. It is well known that there is a southwest-northeast SST dipole pattern in the southern IO named the Indian Ocean Subtropical Dipole (IOSD) mode, which tends to peak in austral summer (Behera & Yamagata, 2001; Morioka et al., 2012; Terray et al., 2004) and is tightly related to variability of the subtropical high pressure system (Morioka et al., 2012). Despite suggestion that SST anomalies over the southeastern tropical IO during austral summer would induce variability of the subtropical high, which may in turn trigger an internal IOD (Fischer et al., 2005), the issue of how the southern IO may affect the IOD remains unknown. Here we show that subtropical high variability and high-latitude activities in the Southern Hemisphere can induce an IOD event, which we refer to as the Southern Hemisphere Mechanism (SHM).

2. Data and Methods

Monthly SST data are provided by Extended Reconstruction SST version 5 (ERSSTv5) with a 2° × 2° resolution (Smith et al., 2008). Monthly atmospheric data including 10-m wind, SLP, and geopotential height are from the National Centers for Environmental Prediction-National Center for Atmospheric Research (NCEP-NCAR) Reanalysis I with a 2.5° × 2.5° resolution (Kalnay et al., 1996). All data sets cover the period from 1950 to 2019. We note that seasonal cycle and long-term trend have been removed from all variables firstly. We also have checked the SST and SLP data from the Met Office Hadley Centre (HadISST and HadSLP) (Allan & Ansell, 2006; Kennedy et al., 2011a, 2011b) and obtained similar results.

The dipole mode index (DMI) is the difference between the area-mean SST anomaly over the western tropical IO (50–70°E, 10°S–10°N) and southeastern tropical IO (90–110°E, 10°S–Eq.) (Saji et al., 1999). The Niño3.4 index is defined as the area-mean SST anomaly over 170–120°W and 5°S–5°N (Trenberth, 1997). The Southern Annular Mode (SAM) index is the difference of the zonal mean of SLP over the 40°S and 65°S (Gong & Wang, 1999).

To remove ENSO influences, this study uses a combined linear regression, highlighting the intrinsic variations in the IO. This method recognizes the ENSO as a dynamical entity, in which both developing and decaying stages of the ENSO have considerable impacts on the IO SST (Xie et al., 2009; Yuan et al., 2011). To achieve the goal, we conduct a three-step recursive linear regression, in which the first step removes the concurrent impact of ENSO on the IO SST, while the second and third steps remove the lead and lagged impacts of ENSO in its developing and decaying years, respectively. Due to the use of lead-lagged regressions, we retain the period of 1951–2018 to ensure the completeness of ENSO cycle. See the Text S1 in supporting information for detailed descriptions.

Since the IOD features a phase-locking nature, we use the seasonal empirical orthogonal function (SEOF) to analyze the SST evolution in the IO (30–130°E, 30°S–10°N). The SEOF can identify not only the spatial patterns but also the temporal evolution of leading variability modes for a selected variable (i.e., SST) (Wang & An, 2005; Weller et al., 2014). Following Wang and An (2005), we firstly convert the temporal evolution of the SST into an "expanded" space matrix and then apply an EOF analysis to the covariance of the matrix. The expanded space matrix is expressed as

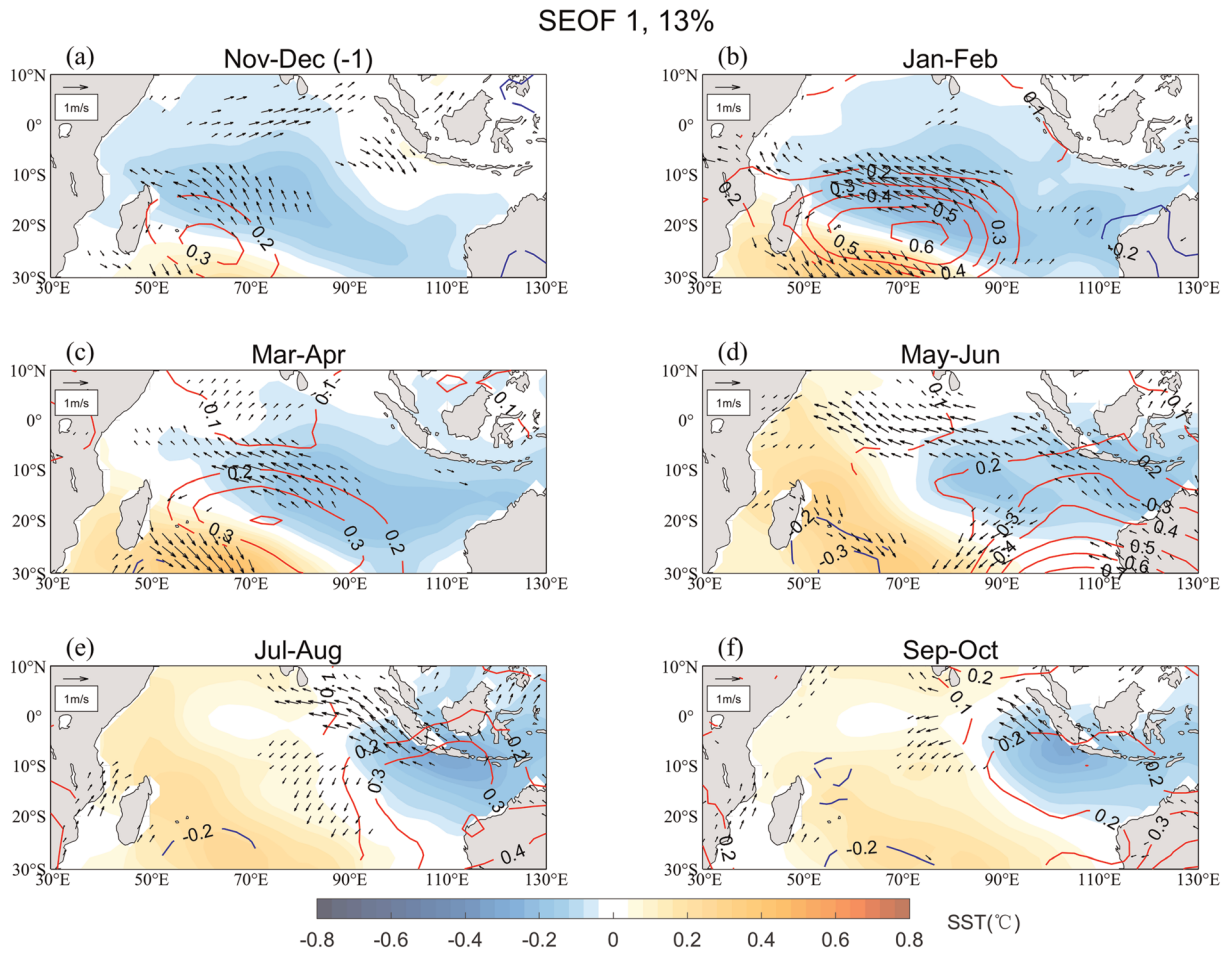

Figure 1. Southern Hemisphere Mechanism (SHM). (a) to (f) show the SHM evolution from previous November–December (donated by −1) to the following September–October, revealed by the first mode of seasonal empirical orthogonal function (SEOF) on bimonthly mean sea surface temperature (SST, shaded) anomalies in the Indian Ocean. The contours (high/low anomaly starts at 0.1/−0.1 hPa with interval of 0.1 hPa shown by red/blue lines) and vectors represent the anomalies of sea level pressure (SLP) and 10-m wind obtained by regressing to the principal component of the first SEOF mode (PC1), respectively. The regressed results exceeding 90% confidence level of Student's *t* test are shown.

$$X(x,\,t)=[x_{ND}(t),x_{JF}(t),x_{MA}(t),x_{MJ}(t),x_{JA}(t),x_{SO}(t)], \tag{1}$$

where X is total samples of the IO SST anomalies, while x represents the subset of X in each calendar month; t is the year from 1951 to 2018; and *ND*, *JF*, *MA*, *MJ*, *JA*, and *SO* denote bimonthly mean of November–December, January–February, March–April, May–June, July–August, and September–October, respectively. In this study, we use bimonthly mean SST anomaly instead of trimonthly from the November–December in the previous year (donated by −1) to the following September–October for covering the period from the SHM developing stage to the IOD peak. Thus, the first sample is in the November–December 1951.

3. The Southern Hemisphere Mechanism

After removing ENSO impacts and applying SEOF onto SST, the first SEOF mode features a connection between the IOSD and the IOD, suggesting a plausible triggering mechanism of the IOD from the Southern Hemisphere, hereafter SHM (Figure 1). By regressing anomalies of atmospheric fields onto the principal component of the first SEOF mode (PC1, Figure S1), we investigate how the atmosphere forces the southern signals evolving into the IOD via the SHM. For reference, we also apply the same processes to the data retaining ENSO impact (Figures S2 and S3) and find that such mechanism appears as the second mode with weaker variance.

The initial SST anomaly features an IOSD-like pattern, where the anomalous cooling appears initially in the central southern IO (centered around 80°E, 20°S) during the previous November–December (Figure 1a). Such anomalous SST pattern peaks in January–February, characterized by positive SST anomalies in the southwest IO and negative SST anomalies in the southeastern IO and is associated with the high pressure anomaly and an anomalous anti-cyclonic wind gyre there (Figure 1b). At the southern flank of anomalous SLP, northwesterly wind anomalies blow against the background easterly winds, while the southeasterly winds at the northern edge enhance the background winds and thus the evaporation to cool SST. This is consistent with the fact that the Mascarene High activities can lead to the IOSD (Morioka et al., 2012).

The eastward movement of the SLP anomalies causes the cool SST anomalies to move toward the Sumatra-Java coast (Figures 1c and 1d). By May–June, SLP and SST anomalies both reach the eastern boundary of the IO (Figure 1d). The positive SLP anomalies over the southwest Australian coast accompany the anti-cyclonic winds to the southeastern IO, leading to a stronger-than-normal monsoon off Sumatra-Java (Figure 1d). At this stage, the southeasterly wind anomalies over the southeastern tropical IO cause anomalous cooling, by enhanced upwelling and latent heat release (Annamalai et al., 2003; Li et al., 2003; Rao et al., 2008). Therefore, the anomalous SST cooling anchors in the southeastern tropical IO and forms the eastern pole of the IOD, appearing much earlier than the typical IOD event (Figures 1d and 1e). At the same time, although the anomalous SST warming moves further to the south (centered around 60°E, 30°S), it also expands equatorward within the western basin and forms the zonal dipole pattern at low latitudes (Figures 1e and 1f). Thus, the subtropical signals have preconditioned favorably for the IOD onset, after which equatorial dynamics comes in to sustain the IOD development.

We use the bimonthly mean of DMI to investigate the relationship between the SHM and the IOD since the PC1 is of an annual interval. The June–July and September–October represent the IOD developing and mature phases, respectively (Figure S1). The PC1 has a stronger correlation with the DMI in June–July than in September–October (0.62 vs. 0.43). It indicates that the SHM is a stronger contributor for the IOD developing stage. The larger difference between the original DMI and the no-ENSO DMI in September–October (increase from 0.43 to 0.53) than in June–July (increase from 0.62 to 0.65) also indicates that the ENSO contribution is larger during the IOD peak phase. For events with an ENSO, such as year 1997–1998, the DMI value becomes lower than one standard deviation after removing the ENSO impacts (Figure S1b). For events without a robust ENSO, such as 1961 and 1977 (Du et al., 2013), the DMI value changes inconspicuously but the PC1 value is large (Figure S1b). These results suggest that internal IO variability can induce an IOD event via this SHM.

It is important to know the reason why the SLP anomalies move eastward. Since high-latitude climatic processes such as the SAM are known to influence the midlatitudes (Cai et al., 2011; Nan et al., 2009; Thompson & Wallace, 2000), we use the correlation coefficient between PC1 and the SAM index, a composite of the SAM index, and composites (positive minus negative SHM) of SLP and wind anomalies to examine how the high-latitude activities involve in the SHM (Figure 2). Both correlation and composite analyses show a negative SAM phase in austral summer (January–February), featured by high pressure anomalies in the polar region, and low pressure anomalies in the subpolar region (Figures 2a and 2b). This negative SAM pattern is accompanied by an anomalous high pressure anchors over the western subtropical IO, showing a meridional tripolar pattern of SLP in the IO section (Figures 1b and 2b). With a phase transition of the SAM (Figure 2a), high pressure anomalies in the subtropical IO related with a positive SAM pattern move and appear over the eastern subtropical IO in the austral winter (July–August) (Figures 1b–1e, 2a, and 2e). The northern edge of such high pressure anomaly, therefore, causes a stronger monsoon with southeasterly wind anomalies in the southeastern tropical IO (Figures 1e, 2d, and 2e). These composite results correspond to the SHM shown in Figure 1. Our analyses so far indicate that, associated with the high-latitude activities, the subtropical high variability induces a SLP eastward movement, which brings southeasterly wind anomalies to the southeastern tropical IO and triggers an IOD event.

4. Associated Changes in IOD Characteristics

We note that the SHM can operate independently from the ENSO since the ENSO impacts have been removed. However, it may be more complex in the actual situation, as observed in 2006 when the ENSO and the Southern Hemisphere were both influential. As such, we discuss their joint effects on the IOD.

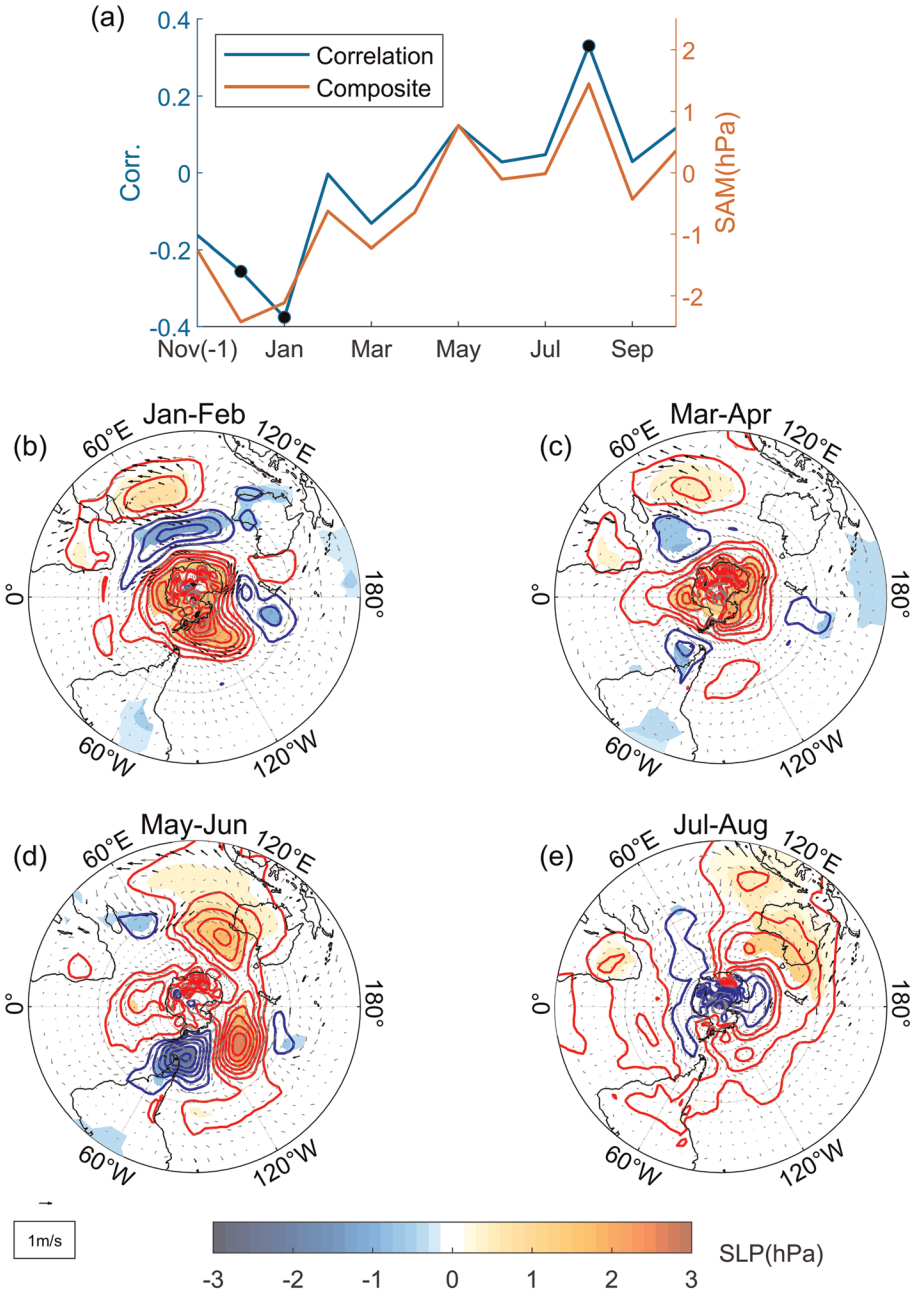

Figure 2. Southern Annular Mode (SAM) and Southern Hemisphere Mechanism (SHM). (a) Blue line indicates the correlation between PC1 of SEOF and the SAM index in each calendar month from November during previous (donated by −1) year to October; orange line indicates the difference in composite of the SAM index between positive SHM cases and negative SHM cases for samples in which PC1 is larger/smaller than 1/−1. (b, c) Composites of SLP (contours) and wind (vectors) anomalies from January–February to July–August of the positive SHM and minus negative SHM years. Anomalous SLP/wind exceeding the 90% confidence level of Student's *t* test are shaded/bold.

The SEOF results including the ENSO signals show that the first SEOF mode (explaining 22% variance) displays the transition from a decaying positive IOD, to an IO basin-wide warming mode, and finally to a negative IOD mode (Figure S2). It reflects the IO capacitor effect of the ENSO cycle (Xie et al., 2009, 2016). However, the IOSD-IOD connection is captured by the second SEOF mode (explaining 11% variance, Figure S3). These results reveal that the ENSO is the dominant factor that affects the IO SST variability, in agreement with past studies.

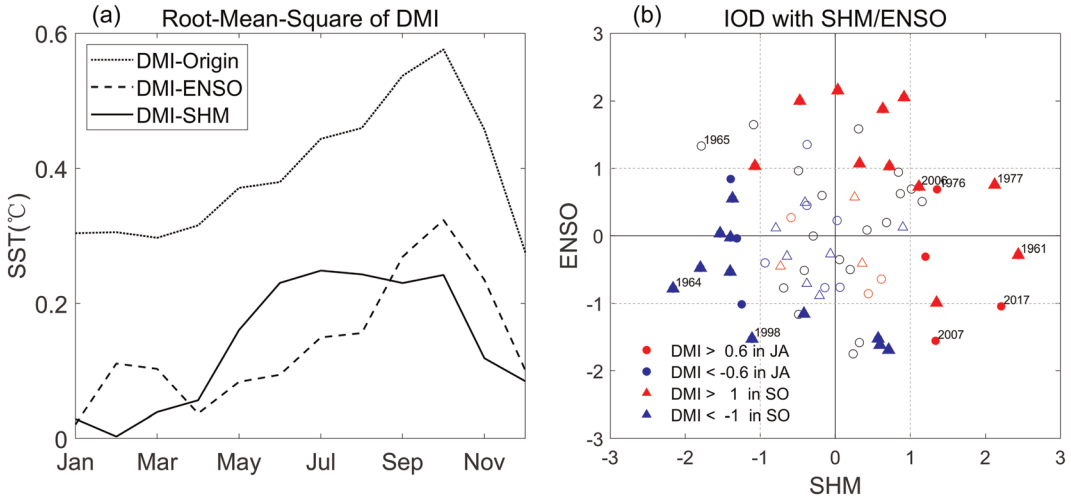

Figure 3. Forcing of the IOD by ENSO and Southern Hemisphere Mechanism (SHM). (a) Seasonal evolution of the IOD shown by root mean square of the DMI in each calendar month. The original DMI (dotted line) includes all kind of influences like ENSO, SHM, and others attributable to ENSO and SHM. The ENSO-induced DMI (dashed line) is calculated by the combined linear regression. The SHM induced (solid) is obtained by linearly regressing the DMI without ENSO influence onto the PC1 of SEOF. (b) Scatter diagram of SHM-ENSO showing their respective influence on the IOD. Red (blue) dots/triangles stand for the positive (negative) IOD with a criterion of DMI exceeding 0.6/1 (−0.6/−1) standard deviation in July–August/September–October. The vertical and horizontal axes indicate the normalized bimonthly mean of the Niño3.4 index during December–January and the PC1 of SEOF, respectively. The symbols are filled when the SHM (ENSO) is exceeding 1/−1 standard deviation. Because the unseasonable IOD is generally weaker than normal, we set the 0.6 standard deviations as the threshold. Note that some events are marked with years on the upper-right corner.

The ENSO influence is at its maximum during the IOD peak season (i.e., from September to November) as the ENSO develops concurrently (Xu & Chan, 2001), while the SHM induces the IOD much earlier starting from May (Figure 3a). During May–August, it explains more variance of the DMI than the ENSO does. This implies that the southern influence is locked to the seasonal cycle of the IO monsoon, which means that the background southeasterly wind is crucial to the IOD development. Hence, different types of IOD lifetime may be due to such southern influence. Some IOD events tend to develop and even peak in June–August, such as prolonged IOD or unseasonable IOD (Du et al., 2013). In these kinds of events, like the events in 1961, 2006 (Horii et al., 2008), and 2017 (Zhang et al., 2018) (Figures S4–S6, see more details in Text S2), the Southern Hemisphere plays a role as revealed by PC1 (above one standard deviation, Figure 3b).

In fact, both the SHM and ENSO can occur in the same year and affect evolution and strength of an IOD event. One such example is the 2006 positive IOD event, which was contributed by both the positive SHM and El Niño (Vinayachandran et al., 2007) (Figure S4). Another example is the strong negative IOD event in 1998, when both the negative phases of SHM and La Niña had contributed (Figure 3b). However, the 2007 positive IOD event, as the second of the consecutive three positive IOD events during 2006–2008, co-occurred with a positive SHM and a weak La Niña (Behera et al., 2008; Luo et al., 2008; Rao et al., 2008). As a result, it underwent a typical evolution of the unseasonable IOD and only lasted for a short period of time. The 2017 positive event was also similar, which developed from the southern IO, but the concurrent La Niña contributed to its earlier termination (Zhang et al., 2018). A similar example is the negative IOD in 1965. The negative phase of SHM led to this IOD, but its development was interrupted by an El Niño. Therefore, the SHM and ENSO sometimes offset and led to weak and unseasonable IOD events with an earlier termination, but sometimes they conspire leading to strong and prolonged IOD events. Nevertheless, there are still some IOD events that develop without the SHM or the ENSO (Figure 4b), suggesting that there are other triggering mechanisms.

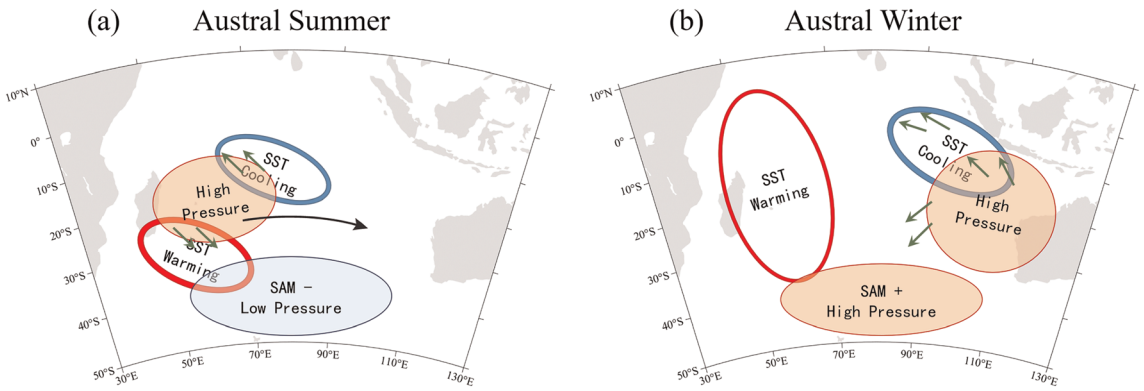

Figure 4. Schematic diagram of the Southern Hemisphere Mechanism (SHM). (a) and (b) display the SHM evolution in austral summer and winter, respectively. Reddish/bluish shadings represent the higher/lower pressure anomalies. Red/blue ovals represent the warmer/cooler sea surface temperature (SST) anomalies. Green vectors represent the wind anomalies. Black arrows show the movement of the pressure anomalies.

5. Discussion

We note that the second SEOF mode explains ~12% proportion of the total variance and exhibits a pattern like the Ningaloo Niño/Niña mode (Figure S7) (Feng et al., 2013; Kido et al., 2015). Considering the relatively variance contribution, the Ningaloo Niño/Niña is important in the southern IO (Tozuka et al., 2014). Particularly, the second SEOF mode shows a weak IOD-like condition after July–August (Figures S7e and S7f), indicating a weak relationship with the IOD.

The IOSD occasionally revives in the second year after an incomplete demise (Behera & Yamagata, 2001). We suggest that if the subtropical high anomaly persists in the southern IO, the IOD could recur through the SHM, for example, the 1976–1977 and 2006–2007 positive events (also in 1964–1965 negatively but the 1965 event was aborted). The 2006 and 2007 positive IOD events successfully predicted by Luo et al. (2008) are captured by the first SEOF mode of this study. Considering the subtropical impact on the tropics, this SHM can be used to improve the predictability of the IOD events (Tanizaki et al., 2017). Nevertheless, the relationship between the IOD and high-latitude climate variability is still under debate. In this regard, some studies found that the SAM is not a driver of the IOD based on the model simulations (Cai et al., 2011). Here, we hypothesize that the SAM does not directly influence the IOD, but the phase transition of the SAM may cause subtropical high variability in the southern IO and further influence the tropics (Nan et al., 2009). This hypothesis awaits future tests using a model experiment.

As a subtropical climate mode in the Pacific, the Seasonal Footprinting Mode is known to affect the tropical SST and induce the ENSO variability (Chiang & Vimont, 2004; Vimont et al., 2003; Yu et al., 2010). With this mechanism, the SST anomaly extends equatorward from the northeastern Pacific one to two seasons before the ENSO onsets, via the wind-evaporation-SST feedback (Xie & Philander, 1994; Yu & Fang, 2018). However, the SHM in the IO is different from the Seasonal Footprinting Mode with much weaker wind-evaporation-SST feedback involved. The anomalous subtropical high and southeasterly winds force the SST to evolve and to reach the tropics, rather than the interactions of the near-equatorial SST with the atmosphere.

6. Conclusion

This study proposes a novel triggering mechanism of the IOD from the Southern Hemisphere (Figure 4). We show a development of SST cooling anomaly from the southern IO to the tropics, accompanied by an eastward movement of an anomalous subtropical high system (Figure 4a). As the background southeasterly winds associated with the monsoon in the southeastern IO move equatorward, the anomalous southeasterly winds during May–June lead to a much earlier SST cooling over the southeastern tropical IO (Figure 4b). The eastward movement of the high pressure anomaly over the subtropical IO is important in the SHM, which enhances the monsoon off Sumatra-Java during May–August and is related to the phase transition of SAM. This SHM can operate independently from the ENSO. Its impact on the IOD mainly starts from May to June and persists until the IOD peak season. This explains why some IOD events develop and even mature in austral winter. In particular, the present study emphasizes the role of tropical-subtropical

connection in the generation of the IOD and that the high latitude is possibly involved in tropical climate variability, with implication for improvement of the IOD predictability.

Data Availability Statement

We acknowledge the NOAA/OAR/ESRL PSL, Boulder, Colorado, USA, for providing ERSST and NCEP-reanalysis data from their Web site (at https://psl.noaa.gov/); HadISST and HadSLP2 data can be downloaded online (from https://www.metoffice.gov.uk/hadobs/).

Acknowledgments

We thank an anonymous reviewer and Dr. Thanh Le for their helpful comments. This study is supported by the National Natural Science Foundation of China (41525019 and 41830538), the Chinese Academy of Sciences (XDB42010304, XDA15020901, 133244KYSB20190031, and ZDRW-XH-2019-2), the State Oceanic Administration of China (GASI-IPOVAI-02), and the Southern Marine Science and Engineering Guangdong Laboratory (Guangzhou) (GML2019ZD0303, GML2019ZD0306, and 2019BT2H594). Lian-Yi Zhang is supported by the University of the Chinese Academy of Sciences (UCAS) Joint PhD Training Scholarship. Wenju Cai is supported by the Centre for Southern Hemisphere Oceans Research, a joint research center between QNLM and CSIRO, and by the Earth Systems and Climate Change Hub of the Australian Government's National Environmental Science Program. Jin-Yi Yu is supported by U.S. National Science Foundation's Climate & Large-scale Dynamics Program under Grant AGS-1833075.

References

Allan, R., & Ansell, T. (2006). A new globally complete monthly historical gridded mean sea level pressure dataset (HadSLP2): 1850–2004. *Journal of Climate*, *19*(22), 5816–5842. https://doi.org/10.1175/JCLI3937.1

Annamalai, H., Kida, S., & Hafner, J. (2010). Potential impact of the tropical Indian Ocean–Indonesian seas on El Niño characteristics. *Journal of Climate*, *23*(14), 3933–3952. https://doi.org/10.1175/2010JCLI3396.1

Annamalai, H., Murtugudde, R., Potemra, J., Xie, S.-P., Liu, P., & Wang, B. (2003). Coupled dynamics over the Indian Ocean: Spring initiation of the zonal mode. *Deep Sea Research Part II*, *50*(12–13), 2305–2330. https://doi.org/10.1016/S0967-0645(03)00058-4

Ashok, K., Guan, Z., & Yamagata, T. (2003). A look at the relationship between the ENSO and the Indian Ocean Dipole. *Journal of the Meteorological Society of Japan*, *81*(1), 41–56. https://doi.org/10.2151/jmsj.81.41

Behera, S. K., Krishnan, R., & Yamagata, T. (1999). Unusual ocean-atmosphere conditions in the tropical Indian Ocean during 1994. *Geophysical Research Letters*, *26*(19), 3001–3004. https://doi.org/10.1029/1999GL010434

Behera, S. K., Luo, J.-J., Masson, S., Rao, S. A., Sakuma, H., & Yamagata, T. (2006). A CGCM study on the interaction between IOD and ENSO. *Journal of Climate*, *19*(9), 1688–1705. https://doi.org/10.1175/JCLI3797.1

Behera, S. K., Luo, J.-J., & Yamagata, T. (2008). Unusual IOD event of 2007. *Geophysical Research Letters*, *35*, L14S11. https://doi.org/10.1029/2008GL034122

Behera, S. K., & Yamagata, T. (2001). Subtropical SST dipole events in the southern Indian Ocean. *Geophysical Research Letters*, *28*(2), 327–330. https://doi.org/10.1029/2000GL011451

Bjerknes, J. (1969). Atmospheric teleconnections from the equatorial Pacific. *Monthly Weather Review*, *97*(3), 163–172. https://doi.org/10.1175/1520-0493(1969)097<0163:ATFTEP>2.3.CO;2

Cai, W., Cowan, T., & Raupach, M. (2009). Positive Indian Ocean Dipole events precondition southeast Australia bushfires. *Geophysical Research Letters*, *36*, L19710. https://doi.org/10.1029/2009GL039902

Cai, W., Pan, A., Roemmich, D., Cowan, T., & Guo, X. (2009). Argo profiles a rare occurrence of three consecutive positive Indian Ocean Dipole events, 2006–2008. *Geophysical Research Letters*, *36*, 08701. https://doi.org/10.1029/2008GL037038

Cai, W., & Qiu, Y. (2013). An observation-based assessment of nonlinear feedback processes associated with the Indian Ocean Dipole. *Journal of Climate*, *26*(9), 2880–2890. https://doi.org/10.1175/JCLI-D-12-00483.1

Cai, W., Sullivan, A., & Cowan, T. (2011). Interactions of ENSO, the IOD, and the SAM in CMIP3 models. *Journal of Climate*, *24*(6), 1688–1704. https://doi.org/10.1175/2010JCLI3744.1

Cai, W., Zheng, X., Weller, E., Collins, M., Cowan, T., Lengaigne, M., et al. (2013). Projected response of the Indian Ocean Dipole to greenhouse warming. *Nature Geoscience*, *6*(12), 999–1007. https://doi.org/10.1038/ngeo2009

Chiang, J. C. H., & Vimont, D. J. (2004). Analogous Pacific and Atlantic meridional modes of tropical atmosphere–ocean variability. *Journal of Climate*, *17*(21), 4143–4158. https://doi.org/10.1175/JCLI4953.1

Crétat, J., Terray, P., Masson, S., & Sooraj, K. P. (2017). Intrinsic precursors and timescale of the tropical Indian Ocean Dipole: Insights from partially decoupled numerical experiment. *Climate Dynamics*, *51*(4), 1311–1332.

Delman, A. S., Sprintall, J., McClean, J. L., & Talley, L. D. (2016). Anomalous Java cooling at the initiation of positive Indian Ocean Dipole events. *Journal of Geophysical Research: Oceans*, *121*, 5805–5824. https://doi.org/10.1002/2016JC011635

Drbohlav, H.-K. L., Gualdi, S., & Navarra, A. (2007). A diagnostic study of the Indian Ocean Dipole mode in El Niño and non–El Niño years. *Journal of Climate*, *20*(13), 2961–2977. https://doi.org/10.1175/JCLI4153.1

Du, Y., Cai, W., & Wu, Y. (2013). A new type of the Indian Ocean Dipole since the mid-1970s. *Journal of Climate*, *26*(3), 959–972. https://doi.org/10.1175/JCLI-D-12-00047.1

Endo, S., & Tozuka, T. (2015). Two flavors of the Indian Ocean Dipole. *Climate Dynamics*, *46*(11–12), 3371–3385.

Feng, M., McPhaden, M. J., Xie, S.-P., & Hafner, J. (2013). La Niña forces unprecedented Leeuwin Current warming in 2011. *Scientific Reports*, *3*(1), 1277. https://doi.org/10.1038/srep01277

Fischer, A. S., Terray, P., Guilyardi, E., Gualdi, S., & Delecluse, P. (2005). Two independent triggers for the Indian Ocean Dipole/Zonal mode in a coupled GCM. *Journal of Climate*, *18*(17), 3428–3449. https://doi.org/10.1175/JCLI3478.1

Gong, D., & Wang, S. (1999). Definition of Antarctic Oscillation index. *Geophysical Research Letters*, *26*(4), 459–462. https://doi.org/10.1029/1999GL900003

Guo, F., Liu, Q., Sun, S., & Yang, J. (2015). Three types of Indian Ocean Dipoles. *Journal of Climate*, *28*(8), 3073–3092. https://doi.org/10.1175/JCLI-D-14-00507.1

Horii, T., Hase, H., Ueki, I., & Masumoto, Y. (2008). Oceanic precondition and evolution of the 2006 Indian Ocean dipole. *Geophysical Research Letters*, *35*, L03607. https://doi.org/10.1029/2007GL032464

Izumo, T., Vialard, J., Lengaigne, M., de Boyer Montegut, C., Behera, S. K., Luo, J.-J., et al. (2010). Influence of the state of the Indian Ocean Dipole on the following year's El Niño. *Nature Geoscience*, *3*(3), 168–172. https://doi.org/10.1038/ngeo760

Kalnay, E., Kanamitsu, M., Kistler, R., Collins, W., Deaven, D., Gandin, L., et al. (1996). The NCEP/NCAR 40-year reanalysis project. *Bulletin of the American Meteorological Society*, *77*(3), 437–471. https://doi.org/10.1175/1520-0477(1996)077<0437:TNYRP>2.0.CO;2

Kennedy, J. J., Rayner, N. A., Smith, R. O., Parker, D. E., & Saunby, M. (2011a). Reassessing biases and other uncertainties in sea surface temperature observations measured in situ since 1850: 1. Measurement and sampling uncertainties. *Journal of Geophysical Research*, *116*(D14103), 1–13.

Kennedy, J. J., Rayner, N. A., Smith, R. O., Parker, D. E., & Saunby, M. (2011b). Reassessing biases and other uncertainties in sea surface temperature observations measured in situ since 1850: 2. Biases and homogenization. *Journal of Geophysical Research*, *116*(D14104), 1–22.

Kido, S., Kataoka, T., & Tozuka, T. (2015). Ningaloo Niño simulated in the CMIP5 models. *Climate Dynamics*, *47*(5–6), 1469–1484.
Li, T., Wang, B., Chang, C. P., & Zhang, Y. S. (2003). A theory for the Indian Ocean dipole-zonal mode. *Journal of the Atmospheric Sciences*, *60*(17), 2119–2135. https://doi.org/10.1175/1520-0469(2003)060<2119:ATFTIO>2.0.CO;2
Luo, J.-J., Behera, S. K., Masumoto, Y., Sakuma, H., & Yamagata, T. (2008). Successful prediction of the consecutive IOD in 2006 and 2007. *Geophysical Research Letters*, *35*, L14S02. https://doi.org/10.1029/2007GL032793
Meyers, G., McIntosh, P., Pigot, L., & Pook, M. (2007). The years of El Niño, La Niña, and interactions with the tropical Indian Ocean. *Journal of Climate*, *20*(13), 2872–2880. https://doi.org/10.1175/JCLI4152.1
Morioka, Y., Tozuka, T., & Yamagata, T. (2012). How is the Indian Ocean Subtropical Dipole excited? *Climate Dynamics*, *41*(7–8), 1955–1968.
Moum, J. N., de Szoeke, S. P., Smyth, W. D., Edson, J. B., DeWitt, H. L., Moulin, A. J., et al. (2014). Air–sea interactions from westerly wind bursts during the November 2011 MJO in the Indian Ocean. *Bulletin of the American Meteorological Society*, *95*(8), 1185–1199. https://doi.org/10.1175/BAMS-D-12-00225.1
Nan, S., Li, J., Yuan, X., & Zhao, P. (2009). Boreal spring Southern Hemisphere Annular Mode, Indian Ocean sea surface temperature, and East Asian summer monsoon. *Journal of Geophysical Research*, *114*, D02103. https://doi.org/10.1029/2008JD010045
Qiu, Y., Cai, W., Guo, X., & Ng, B. (2014). The asymmetric influence of the positive and negative IOD events on China's rainfall. *Scientific Reports*, *4*, 4943.
Rao, S. A., Luo, J.-J., Behera, S. K., & Yamagata, T. (2008). Generation and termination of Indian Ocean dipole events in 2003, 2006 and 2007. *Climate Dynamics*, *33*(6), 751–767.
Saji, N. H., Goswami, B. N., Vinayachandran, P. N., & Yamagata, T. (1999). A dipole mode in the tropical Indian Ocean. *Nature*, *401*(6751), 360–363. https://doi.org/10.1038/43854
Saji, N. H., & Yamagata, T. (2003). Possible impacts of Indian Ocean Dipole mode events on global climate. *Climate Research*, *25*(2), 151–169. https://doi.org/10.3354/cr025151
Smith, T. M., Reynolds, R. W., Peterson, T. C., & Lawrimore, J. (2008). Improvements to NOAA's historical merged land-ocean surface temperature analysis (1880–2006). *Journal of Climate*, *21*(10), 2283–2296. https://doi.org/10.1175/2007JCLI2100.1
Sun, S., Lan, J., Fang, Y., Tana, & Gao, X. (2015). A triggering mechanism for the Indian Ocean Dipoles independent of ENSO. *Journal of Climate*, *28*(13), 5063–5076. https://doi.org/10.1175/JCLI-D-14-00580.1
Tanizaki, C., Tozuka, T., Doi, T., & Yamagata, T. (2017). Relative importance of the processes contributing to the development of SST anomalies in the eastern pole of the Indian Ocean Dipole and its implication for predictability. *Climate Dynamics*, *49*(4), 1289–1304. https://doi.org/10.1007/s00382-016-3382-2
Terray, P., Dominiak, S., & Delecluse, P. (2004). Role of the southern Indian Ocean in the transitions of the monsoon-ENSO system during recent decades. *Climate Dynamics*, *24*(2–3), 169–195.
Thompson, D. W. J., & Wallace, J. M. (2000). Annular modes in the extratropical circulation. *Part I: Month-to-month variability, Journal of Climate*, *13*(5), 1000–1016.
Tozuka, T., Kataoka, T., & Yamagata, T. (2014). Locally and remotely forced atmospheric circulation anomalies of Ningaloo Niño/Niña. *Climate Dynamics*, *43*(7–8), 2197–2205. https://doi.org/10.1007/s00382-013-2044-x
Trenberth, K. E. (1997). The definition of El Nino. *Bulletin of the American Meteorological Society*, *78*(12), 2771–2777. https://doi.org/10.1175/1520-0477(1997)078<2771:TDOENO>2.0.CO;2
Vimont, D. J., Wallace, J. M., & Battisti, D. S. (2003). The seasonal footprinting mechanism in the Pacific: Implications for ENSO. *Journal of Climate*, *16*(16), 2668–2675. https://doi.org/10.1175/1520-0442(2003)016<2668:TSFMIT>2.0.CO;2
Vinayachandran, P. N., Kurian, J., & Neema, C. P. (2007). Indian Ocean response to anomalous conditions in 2006. *Geophysical Research Letters*, *34*, L15602. https://doi.org/10.1029/2007GL030194
Vinayachandran, P. N., Saji, N. H., & Yamagata, T. (1999). Response of the equatorial Indian Ocean to an unusual wind event during 1994. *Geophysical Research Letters*, *26*(11), 1613–1616. https://doi.org/10.1029/1999GL900179
Wang, B., & An, S. I. (2005). A method for detecting season-dependent modes of climate variability: S-EOF analysis. *Geophysical Research Letters*, *32*, L15710. https://doi.org/10.1029/2005GL022709
Webster, P. J., Moore, A. M., Loschnigg, J. P., & Leben, R. R. (1999). Coupled ocean-atmosphere dynamics in the Indian Ocean during 1997–98. *Nature*, *401*(6751), 356–360. https://doi.org/10.1038/43848
Weller, E., Cai, W. J., Du, Y., & Min, S. K. (2014). Differentiating flavors of the Indian Ocean Dipole using dominant modes in tropical Indian Ocean rainfall. *Geophysical Research Letters*, *41*, 8978–8986. https://doi.org/10.1002/2014GL062459
Xie, S.-P., Hu, K., Hafner, J., Tokinaga, H., Du, Y., Huang, G., et al. (2009). Indian Ocean capacitor effect on Indo–western Pacific climate during the summer following El Niño. *Journal of Climate*, *22*(3), 730–747. https://doi.org/10.1175/2008JCLI2544.1
Xie, S.-P., Kosaka, Y., Du, Y., Hu, K., Chowdary, J. S., & Huang, G. (2016). Indo-western Pacific ocean capacitor and coherent climate anomalies in post-ENSO summer: A review. *Advances in Atmospheric Sciences*, *33*(4), 411–432. https://doi.org/10.1007/s00376-015-5192-6
Xie, S.-P., & Philander, S. G. H. (1994). A coupled ocean-atmosphere model of relevance to the Itcz in the eastern Pacific. *Tellus Series a-Dynamic Meteorology and Oceanography*, *46*(4), 340–350. https://doi.org/10.3402/tellusa.v46i4.15484
Xu, J., & Chan, J. C. L. (2001). The role of the Asian–Australian monsoon system in the onset time of El Niño events. *Journal of Climate*, *14*(3), 418–433. https://doi.org/10.1175/1520-0442(2001)014<0418:TROTAA>2.0.CO;2
Yang, Y., Xie, S.-P., Wu, L., Kosaka, Y., Lau, N.-C., & Vecchi, G. A. (2015). Seasonality and predictability of the Indian Ocean Dipole mode: ENSO forcing and internal variability. *Journal of Climate*, *28*(20), 8021–8036. https://doi.org/10.1175/JCLI-D-15-0078.1
Yu, J. Y., & Fang, S. W. (2018). The distinct contributions of the seasonal footprinting and charged-discharged mechanisms to ENSO complexity. *Geophysical Research Letters*, *45*, 6611–6618. https://doi.org/10.1029/2018GL077664
Yu, J. Y., Kao, H. Y., & Lee, T. (2010). Subtropics-related interannual sea surface temperature variability in the central equatorial Pacific. *Journal of Climate*, *23*(11), 2869–2884. https://doi.org/10.1175/2010JCLI3171.1
Yu, W. D., Xiang, B. Q., Liu, L., & Liu, N. (2005). Understanding the origins of interannual thermocline variations in the tropical Indian Ocean. *Geophysical Research Letters*, *32*, L24706. https://doi.org/10.1029/2005GL024327
Yuan, D., Wang, J., Xu, T., Xu, P., Hui, Z., Zhao, X., et al. (2011). Forcing of the Indian Ocean Dipole on the interannual variations of the tropical Pacific Ocean: Roles of the Indonesian throughflow. *Journal of Climate*, *24*(14), 3593–3608. https://doi.org/10.1175/2011JCLI3649.1
Zhang, L.-Y., Du, Y., & Cai, W. (2018). A spurious positive Indian Ocean Dipole in 2017. *Science Bulletin*, *63*(18), 1170–1172. https://doi.org/10.1016/j.scib.2018.08.001